

Metallo dendrimers

Synthesis and Substitution Kinetics of Tricarbonylrhenium(I) Dendritic Complexes

Siphelele Malaza,^[a] Preshendren Govender,^[a] Marietjie Schutte-Smith,^[b]
Hendrik G. Visser,^{*[b]} and Gregory S. Smith^{*[a]}

Abstract: Tricarbonylrhenium(I) metallo dendrimers functionalized with *N,N*-2-picolylamino chelates have been synthesized by the [2+1] approach. Methanol substitution reactions of the first- and second-generation poly(propylene amine) tetra- and octanuclear rhenium metallo dendrimers by a range of monodentate nucleophiles (i.e. 4-dimethylaminopyridine, pyridine,

and bromide ions) were investigated and compared to the substitution reactions of an analogous monomeric complex, *fac*-[Re(CO)₃(*N,N*-bidentate)(CH₃OH)]⁺. These detailed kinetic studies reveal that a greater activation is achieved using the metallo dendrimers with no direct interactions between the metal centers.

Introduction

Macromolecules such as dendrimers act as “vehicles” that offer enhanced targeting efficiency via the “enhanced permeability and retention” (EPR) effect.^[1–5] The EPR effect is a phenomenon in which macromolecules accumulate at the tumor site because of an increase in blood vessel permeability within diseased tissues compared to healthy tissues.^[4] The multivalent nature of dendrimers allows for the inclusion of a diverse range of metals for chemotherapy or metallic radionuclides to deliver radiotherapy and diagnostic imaging for follow-up treatment, surgical biopsy guidance and automated pathologic analysis of cancer biopsies and surgical samples.^[5] Technetium-99m (γ -emitting radionuclide) labelling of higher generation dendrimers is an effective approach in evaluating organ distribution studies of drug carriers for therapy and diagnosis.^[6–10] However, exploratory chemical synthesis of technetium-99m complexes in developmental chemistry is limited by the lack of nonradioactive isotopes of Tc. Thus, complexes of nonradioactive rhenium, which is a technetium congener, are often used as ^{99m}Tc models.^[11]

Rhenium and technetium have similar ionic radii, and their *fac*-[M(CO)₃X]⁺ (where M = ^{99m}Tc^I or Re^I; X = halide) containing complexes are often isostructural and relatively similar in chemical reactivity (although they require different reaction conditions).^[11,12] It is also possible to use β -emitting rhenium isotopes (¹⁸⁶Re and ¹⁸⁸Re) for radiotherapy applications.^[13] The low-spin d⁶ *fac*-[M(CO)₃]⁺ (where M = Mn^I, ^{99m}Tc^I, and Re^I) fragment is lipophilic in nature, chemically robust compared to pure

organic molecules, and maintains its structural integrity under harsh conditions.^[11–16] In addition to its kinetic stability, its kinetic behavior is an aspect worth considering, as it can influence the uptake and clearance of radiopharmaceutical agents.

The *fac*-[Re(CO)₃(OH₂)₃]⁺ synthon is an attractive synthon that has great stability in water and the ability to exchange labile solvent ligands. Various synthetic strategies have emerged to substitute the labile aqua ligands of *fac*-[Re(CO)₃(OH₂)₃]⁺, from the use of tridentate ligands to a combination of mono- and bidentate ligands, also known as the [2+1] mixed-ligand approach.^[17,18] As described by Mundwiler et al., the [2+1] approach comprises a bidentate ligand (displacing two of the aqua ligands of the *fac*-[Re(CO)₃(OH₂)₃]⁺ entity) which can influence the overall lipophilicity of the tricarbonyl complex, whilst the third [+1] aqua site is occupied by a monodentate ligand (acting as a linker to a biomolecule).^[18] The advantage of a [2+1] mixed-ligand complexation is that the apical [+1] site can be changed to modulate the physical characteristics of a compound, such as solubility, lipophilicity, and permeability. The integrity of mononuclear complexes achieved via the [2+1] approach has been investigated with *fac*-[Re(CO)₃(*N,N*-bidentate)(OH₂)₂]⁺ functionalized model complexes.^[19–25] It was shown in these studies, that the choice of bidentate ligand has a huge effect on the rate of substitution, with an increase of up to 20 000 times being achieved when moving from an *N,N*-donor like bipyridine to an *O,O*-donor like 3-hydroxyflavone. In vivo, monodentate nucleophiles of varying basicity are ubiquitous and can readily compete for the “labile” aqua coordination site in potential *fac*-[^{99m}Tc(*N,N*-bidentate)-(CO)₃(OH₂)₂]⁺ functionalized radiopharmaceuticals. The substitution kinetics of molecules containing more than one metal center depends on the symmetry of the molecule and the distance between the metal centers, as was reported by van Eldik and others in dinuclear platinum(II) complexes.^[26,27] However, the substitution kinetics of dendrimers have not been examined in great detail.

[a] Department of Chemistry, University of Cape Town, Rondebosch, 7701 Cape Town, South Africa
E-mail: gregory.smith@uct.ac.za
www.gregsmith-research.co.za

[b] Department of Chemistry, University of the Free State, P. O. Box 339, Bloemfontein 9300, South Africa
E-mail: visserhg@ufs.ac.za

Supporting information and ORCID(s) from the author(s) for this article are available on the WWW under <https://doi.org/10.1002/ejic.201700661>.

Herein, we report a series of first- and second-generation poly(propylene amine) metallodendrimers of the type $fac-[Re(CO)_3(N,N\text{-bidentate})X]^n$ (where $X = Br$ ($n = 0$) or OH_2 ($n = +1$)). Furthermore, to the best of our knowledge, this is the first kinetic substitution studies involving metallodendrimers, and more specifically, the first- and second-generation $fac-[Re(CO)_3(N,N\text{-bidentate})(OH_2)]^+$ functionalized metallodendrimers, focusing on the rate of substitution of the apical $[+1]$ aqua ligand by a series of neutral and charged monodentate ligands, with the aim to systematically study the influence on the reactivity of the metal center towards substitution.

Results and Discussion

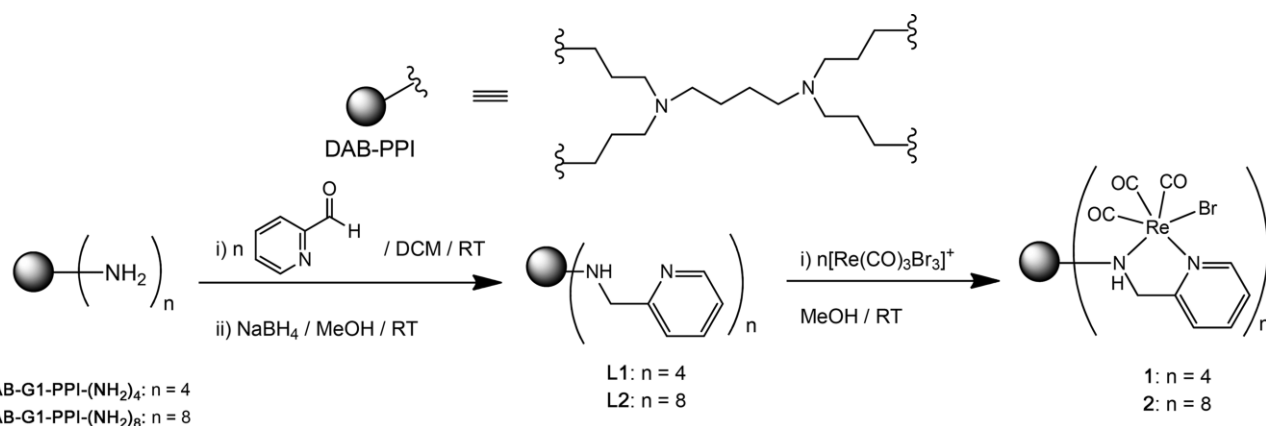
Synthesis of Ligands (**L1** and **L2**) and Rhenium(I)–Bromide Complexes (**1–3**)

The synthesis of suitable chelating N,N -donor periphery-modified dendrimers (**L1** and **L2**) for coordination to Re was achieved via a reductive amination reaction of 2-pyridinecarboxaldehyde with either the first-generation dendritic scaffold DAB–G1–PPI– $(NH_2)_4$ (for **L1**) or the second-generation dendritic scaffold DAB–G2–PPI– $(NH_2)_8$ (for **L2**) (Scheme 1). The water-soluble dendritic ligands **L1** and **L2** were isolated as brown oils and further purified by reverse-phase column chromatography. The monomeric ligand **L3** and its corresponding mononuclear complex **3** (Scheme 2) were prepared as models of the larger dendritic ligands and metallodendrimers.

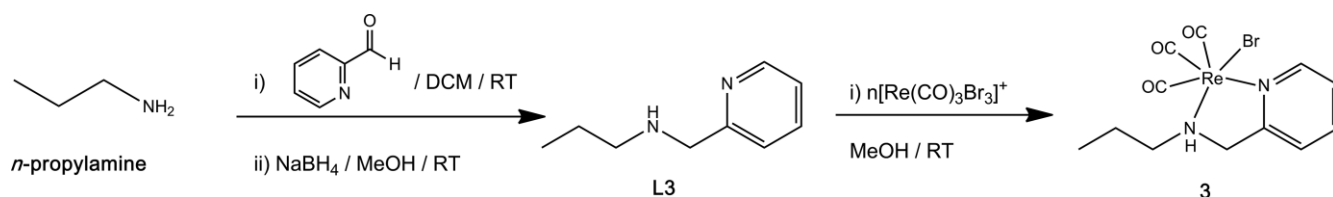
Evidence of the reductive amination reaction is confirmed by a singlet resonance peak at about 3.8 ppm in the 1H NMR spec-

tra for **L1** (Figure S1), **L2** (Figure S2), and **L3**, and is assigned to the enantiotopic methyl protons adjacent to the pyridyl ring(s). The 1H NMR spectra for **L1** and **L2** is characterized by broad overlapping multiplets between 0.8–3.0 ppm, assigned to the aliphatic protons of the dendrimer framework (i.e. protons of the dendritic core and arms). The $^{13}C\{^1H\}$ NMR spectroscopic data reveals a singlet in the range of 52–55 ppm and is assigned to the sp^3 carbon atom of the methyl group adjacent to the pyridyl ring, further confirming successful reduction of the pre-formed imine bond. In addition to the 1H and $^{13}C\{^1H\}$ NMR spectra, strong absorption band(s) at about 1590 cm^{-1} were observed in the IR spectra of **L1–L3** and are assigned to the C=N stretching vibration of the pyridyl ring.

Tricarbonylrhenium(I) complexes are commonly obtained either from $fac-(Et_4N)_2[Re(CO)_3X_3]$ ($X = \text{halogen}$), or a $fac-[Re(CO)_3]^+$ precursor, as reported by Alberto et al.,^[26] or from $fac-[Re(CO)_3(OH_2)_3]^+$ under acidic conditions. The $fac-[Re(CO)_3Br]$ functionalized tetranuclear (**1**), octanuclear (**2**), and mononuclear (**3**) complexes were synthesized by reacting the ligands **L1–L3** with stoichiometric amounts of $fac-(Et_4N)_2[Re(CO)_3Br_3]$ in dry methanol (Scheme 1 and Scheme 2). Metallodendrimers **1** and **2** were isolated as brown solids, and were purified by washing with water. When compared to the 1H NMR spectra of the “metal-free” ligands **L1–L3**, the 1H NMR spectra of **1** (Figure S3), **2** (Figure S4), and **3** (Figure S5) display broadened and a general downfield shift in signals, and further suggests that complexation has occurred. Moreover, the singlet resonance previously assigned to the enantiotopic methylene protons of the dendritic ligands **L1** and **L2**, becomes diastereotopic following complexation and splits into two broad multiplets between 4.7 to 5.2 ppm. Three carbonyl carbon ($C\equiv O$)



Scheme 1. Synthesis of dendritic ligands **L1** and **L2**, and $fac-[N,N\text{-Re}(\text{CO})_3\text{Br}]$ functionalized metallodendrimers **1** and **2**.



Scheme 2. Synthesis of monomeric ligand **L3** and $fac-[N,N\text{-Re}(\text{CO})_3\text{Br}]$ functionalized mononuclear complex **3**.

resonances at approximately 191, 196, and 198 ppm are observed in the $^{13}\text{C}\{^1\text{H}\}$ NMR spectra of **1** (Figure S6), **2** (Figure S7), and **3**, and, in addition to the IR data, further confirm the presence and geometric orientation of the *fac*-[Re(CO) $_3$] $^+$ entity.

X-ray Crystallography

The molecular structure of the model mononuclear complex **3** was elucidated by single-crystal X-ray diffraction and is illustrated in Figure 1. Table S1 summarizes the crystal data and

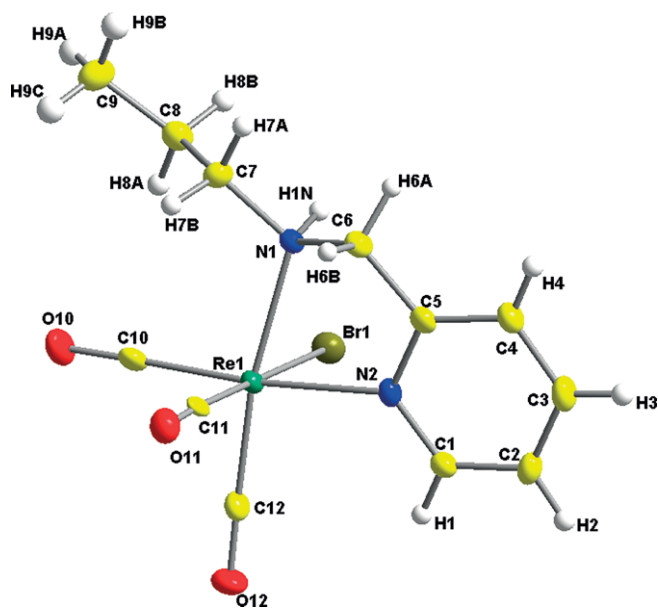


Figure 1. Molecular structure of mononuclear complex **3**, with thermal ellipsoids at the 50 % probability level.

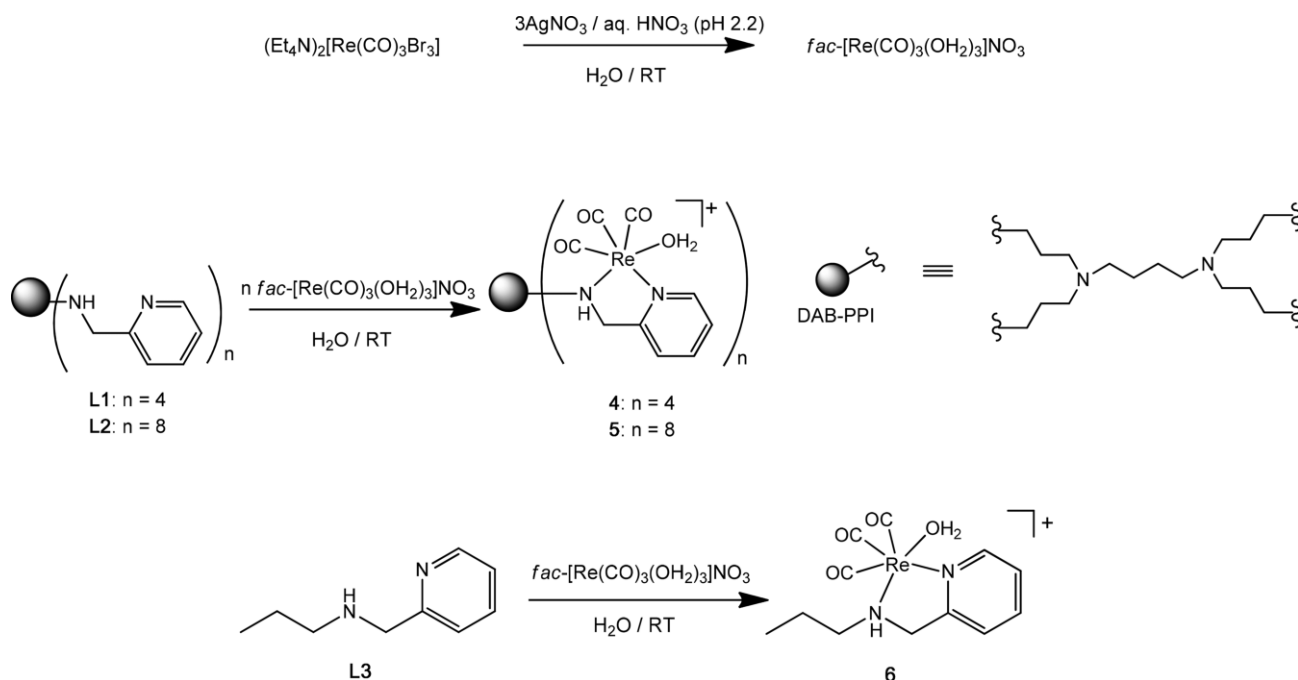
refinement parameters, and Table S2 lists selected bond lengths and angles of **3**.

Mononuclear complex **3** crystallizes in the monoclinic space group, $P2_1/c$, with four formula units per unit cell ($Z = 4$), with each asymmetric unit containing one independent molecule. The ^1H NMR spectrum of **3** (Figure S5) supports the presence of H1N (around 5 ppm). Furthermore, the crystal structure of **3** confirms the *facial* arrangement of the three CO ligands together with the *pseudo* octahedral geometry around the metal center.

The molecular structure of complex **3** shows that the central rhenium atom is coordinated via the two nitrogen atoms of **L3** to form a five-membered ring. The *trans* angles assigned to the rhenium–CO [i.e. C(10)–Re(1)–N(2), C(11)–Re(1)–Br(1), C(12)–Re(1)–N(1)] range between 171.56(18)–179.24(14) $^\circ$, resulting in a slight deviation from the anticipated octahedral limit of 180 $^\circ$. Instead of the expected angle of 90 $^\circ$, the N(2)–Re(1)–N(1) chelate angle of 75.17(16) $^\circ$, delineates the formation of a geometrically strained five-membered ring which contributes significantly to the angular distortion of the octahedral complex **3**. The structure is stabilized by an intermolecular C–H \cdots O hydrogen bond which is formed between one of the hydrogen atoms of the pyridine moiety and the carbonyl oxygen of a neighboring molecule (O12).

Synthesis of Rhenium(I)–Aqua Complexes 4–6

The organometallic precursor *fac*-[Re(CO) $_3$ (OH $_2$) $_3$]NO $_3$, was prepared by stirring *fac*-(Et $_4$ N) $_2$ [Re(CO) $_3$ Br $_3$] in an aqueous solution of HNO $_3$ (pH 2.2) in the presence of silver nitrate (Scheme 3). The substitution reaction produces Et $_4$ N $^+$ as a side product, which shows a similar polarity to the desired complexes and renders the purification of these systems difficult. The acidic



Scheme 3. Synthesis of aqua-derived metallodendrimers **4** and **5**, and mononuclear complex **6**.

reaction conditions serve to minimize dimerization of the organometallic precursor $fac\text{-}[\text{Re}(\text{CO})_3(\text{OH}_2)_3]^+$, and its formation is triggered under basic conditions that result in deprotonation of the aqua ligands to form bridging hydroxide ligands ($\text{Re}\text{-OH}\text{-Re}$).^[28,29] The reaction between $fac\text{-}[\text{Re}(\text{CO})_3(\text{OH}_2)_3]\text{NO}_3$ and stoichiometric amounts of **L1** – **L3** in water, afforded the aqua-derived complexes **4**–**6** (Scheme 3) as either a colorless or brown oil. Complexes **4**–**6** were lyophilized to minimize the water content, required for suitable characterization.

¹H NMR spectra similar to that of the rhenium(I)–bromide complexes **1**–**3** were obtained for the aqua-derived complexes **4**–**6**. However, there is significant peak broadening and coalescing of signals observed in the ¹H NMR spectra for the aqua-derived metallodendrimers **4** and **5**. This is due in part to the multivalent nature of the metallodendrimers, and the line broadening is a consequence of the enhanced relaxation time, which affords the observation of instantaneous NMR signals from all possible orientations of the molecule in solution, instead of the averaged signals normally observed for protracted relaxation events.^[30–32] Compared to the IR spectra of the “metal-free” dendritic ligands **L1** and **L2**, which show the pyridyl C=N absorption band at about 1590 cm⁻¹, the IR spectra of the aqua-derived metallodendrimers **4** and **5** reveal the pyridyl C=N absorption peaks at higher wavenumbers of about 1620 cm⁻¹. This feature was similarly observed in the IR spectrum for the mononuclear aqua-derived complex **6**. Furthermore, the IR spectral analysis revealed two absorption bands at about 2020 and 1860 cm⁻¹ attributed to the symmetric A1 and the asymmetric E stretching vibrations of the carbonyl ligands. The positively charged complexes display higher frequencies than their corresponding neutral complexes, where the carbonyls act as π -acceptors.^[33] Jansen et al. have previously reported on the capability of dendritic architectures to encapsulate small molecules by forming a dendritic box through free rotation and folding of the dendritic arms.^[34] Thus, the elemental analysis data of the metallodendrimers support inclusion of solvent molecules.

Substitution Experiments with Metallodendrimers **4** and **5**

Investigations were performed to confirm methanol substitution on the metallodendrimers. The dendritic aqua-derived metallodendrimers **4** and **5** were dissolved in methanol, to afford MeOH-derived metallodendrimers by displacing the aqua ligand. Such observations have been reported with structurally similar tricarbonylrhenium(I) complexes,^[19–24] achieved via the [2+1] approach. The MeOH-derived metallodendrimers **4** and **5** were further reacted with a neutral monodentate ligand DMAP, displacing the MeOH ligand. The IR absorption bands corresponding to the carbonyl ligands of **4** and **5** in methanol and in the presence of DMAP are listed in Table 1.

The IR data of the complexes **4** and **5** (Table 1) attest to the lability of the [+1] aqua ligand. The displacement of the aqua ligand by MeOH affords three CO absorption bands, whereas in the presence of DMAP, two CO absorption bands are revealed in the IR spectra of the DMAP-derived complexes **4** and **5**. The IR spectroscopy results illustrate that the *N,N*-picoyl chelate is

Table 1. IR data for the CO-stretching vibrations of **4** and **5** in MeOH and DMAP.

Complex	νCO [cm ⁻¹] (in MeOH)	νCO [cm ⁻¹] (in DMAP)
4	2022, 2000, 1870	2022, 1898
5	2022, 1999, 1872	2021, 1898

a weaker σ -donor and/or π -acceptor ligand than the CO ligand. In addition, the IR spectra of the complexes support the integrity of the chelate around the Re^I metal center as the dissociation of the bidentate ligand [+2] could not be observed, as confirmed by the pyridyl C=N absorption band at about 1641 cm⁻¹ in the IR spectra of both DMAP-derived complexes **4** and **5**. As the ligand strength is enhanced, the π -backdonation becomes stronger and the CO bond order is reduced, which results in a decrease in the CO stretching frequencies, explaining the increase of wavenumbers in charged complexes (**4**–**6**) relative to those in neutral complexes (**1**–**3**).^[23]

Substitution Kinetics

The substitution kinetics in complexes **4**, **5**, and **6** of methanol by a range of monodentate ligands using pyridine, DMAP, and Br⁻ ions was then studied in detail. Firstly, it has been shown in the previous section that water is displaced by methanol upon dissolution. Also, our preliminary experiments confirmed that the reactions of all the metal complexes with monodentate ligands involve only one reaction (Figure 2). Figure 2 shows an example of a typical time-resolved absorbance change scan, which was observed for all substitution reactions in this study. This may then be fitted to single exponentials (inset in Figure 2), confirming first-order behavior. All subsequent plots of k_{obs} vs. ligand concentration yielded straight lines. The stability of all the complexes in methanol was established by monitoring solutions over several days using a UV/Vis spectrophotometer. The concentration dependence of the *pseudo*-first-order rate con-

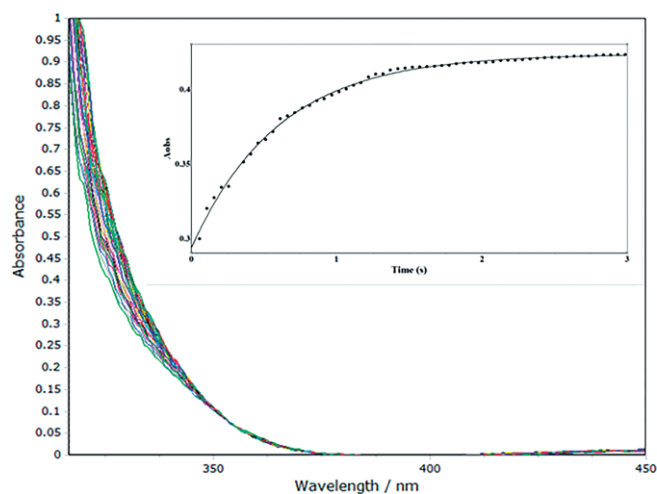


Figure 2. Typical UV/Vis spectral change for the coordinated methanol substitution reaction of $fac\text{-}[\text{Re}(\text{CO})_3(2,4\text{-dPicoH})(\text{MeOH})]$ with DMAP; $[\text{DMAP}] = 0.05 \text{ M}$, 25.0 °C. The inset shows fit of absorbance vs. time data to first-order exponential at 330 nm.

stant (k_{obs}) for the substitution processes of the methanol ligand in $\text{fac}[\text{ReN}(\text{pyridine-2-ylmethyl})\text{propan-1-amine}(\text{CO})_3(\text{MeOH})]^+$ complexes by monodentate entering ligands (denoted by X) is given by Equation (1).

The reactions of **6**, after dissolving it in methanol to form the corresponding methanolato complex, with pyridine and dimethylaminopyridine were followed at four different temperatures with the entering ligand in large excess in each case. The reactions with Br^- ions were only followed at 25.0 °C for comparison. Figure 3 illustrates a typical plot of k_{obs} vs. pyridine concentration at different temperatures after fitting absorbance vs. time plots to Equation (1).



$\text{N},\text{N}'\text{-Bid} = \text{N},\text{N}'\text{-donor ligand}$, X = Py, DMAP, Br^- , n = +1, 0

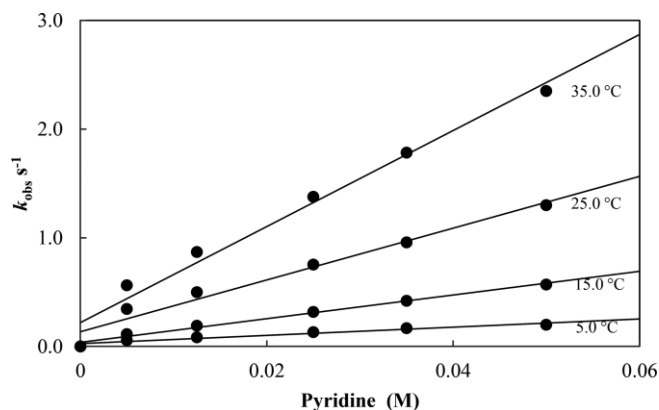


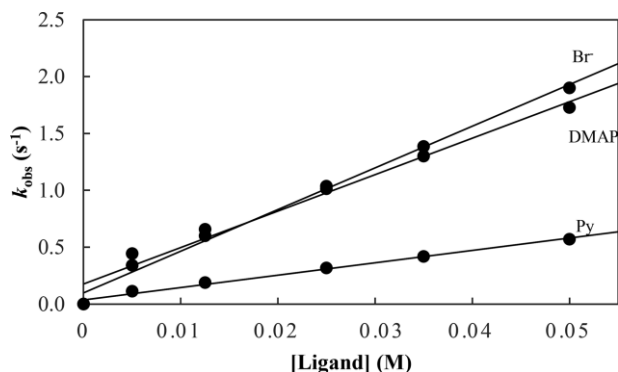
Figure 3. Plot of k_{obs} vs. [py] at 5.0, 15.0, 25.0, and 35.0 °C. [6] = 5.00×10^{-4} M and [py] = 0.005–0.05 M, methanol, $\lambda = 317$ nm.

The rate and equilibrium constants for the reactions of **6** with pyridine, DMAP, and Br^- are reported in Table 2, together with the activation parameters which were obtained from the Eyring equation for the reactions with pyridine and DMAP (see Supporting Information for Eyring plots, Figures S8 and S9). Fig-

Table 2. Rate and equilibrium data for the reactions between **6** and py, DMAP, and Br^- and activation parameters for the reactions between **6** and py and DMAP.

	k_1 [$\text{M}^{-1} \text{s}^{-1}$]	k_{-1} [s^{-1}]	K_1 [M^{-1}]	ΔS^\ddagger [$\text{J K}^{-1} \text{mol}^{-1}$]	ΔH^\ddagger [kJ mol^{-1}]
Pyridine					
5.0 °C	1.80(1)	0.025(7)	72(1)		
15.0 °C	3.68(3)	0.0382(1)	96.3(6)		
25.0 °C	10.2(1)	0.062(4)	164(7)	-34.1(10)	57(3)
35.0 °C	20.4(5)	0.24(3)	85(3)		
DMAP					
5.0 °C	8.57(7)	0.202(8)	42.4(4)		
15.0 °C	13.81(9)	0.287(4)	48.0(9)		
25.0 °C	28.7(1)	0.301(3)	95.3(6)	-79.1(9)	40(2)
35.0 °C	51.9(4)	0.322(9)	161(9)		
Br^-					
25.0 °C	34.8(4)	0.165(1)	211(2)		

ure 4 represents a fit of k_{obs} vs. ligand concentration for all three the reactions at 25.0 °C.



(1) Figure 4. Plot of k_{obs} vs. [ligand] for the reaction between **6** and py, DMAP, and Br^- at 25.0 °C. [6] = 5.00×10^{-4} M, [ligand] = 0.005–0.05 M.

At 25.0 °C, the second-order rate constant, k_1 , for the reactions of **6** with DMAP and Br^- is almost a factor of 3 faster than the comparative reactions with pyridine [$k_1(\text{Br}^-) = 34.8(4)$; $k_1(\text{DMAP}) = 28.7(1)$ and $k_1(\text{py}) = 10.2(1) \text{ M}^{-1} \text{ s}^{-1}$ respectively, at 25.0 °C]. This could be attributed to the favorable charge-charge interactions between the Br^- ion and the corresponding cationic complex and the increased basicity of the entering ligand DMAP ($\text{p}K_a = 9.80$) as opposed to pyridine ($\text{p}K_a = 5.23$).

The stability constants, K_1 , for the formation of $\text{fac}[\text{ReN}(\text{pyridine-2-ylmethyl})\text{propan-1-amine}(\text{CO})_3(\text{Br})]$ is in general higher than that obtained for the corresponding pyridine and DMAP complexes and is similar to what was found in previous reports.^[19–24]

This data, together with the high negative values obtained for ΔS^\ddagger , suggests that these reactions proceed most likely through an I_a type mechanism and corresponds to previous results obtained for similar reactions.^[19–24]

Preliminary stability and kinetic studies of $\text{fac}[\text{Re}_4(\text{N},\text{N}'\text{-G}_1\text{picolyl})(\text{CO})_{12}(\text{OH}_2)_4]^{4+}$ (**4**) and $\text{fac}[\text{Re}_8(\text{N},\text{N}'\text{-G}_2\text{picolyl})(\text{CO})_{24}(\text{OH}_2)_8]^{8+}$ (**5**) with py, DMAP, and Br^- , after obtaining the corresponding methanol complexes, were performed in dry methanol. All the reactions were found to be too fast for conventional UV/Vis spectroscopic studies and could only be followed using a stopped-flow apparatus. Under *pseudo*-first-order conditions, only one reaction was observed for all the reactions studied, and the rates of these reactions increased systematically with the increase in ligand concentration.

If one considers that the rhenium metal centers are removed from each other by at least ten atoms in these structures, and considering the symmetry of the dendrimers, it can be reasoned that the substitution processes will occur simultaneously at all the metal centers. This has also been observed in the substitution reactions involving dinuclear platinum(II) complexes.^[26,27] The time-dependent spectra observed for all the complexes match perfectly to a single exponential fit, and the resulting k_{obs} vs. ligand concentration data could thus be fitted to Equation (1) to yield the second-order rate constants. The data is presented in Table 3. A representative plot of k_{obs} vs. pyridine concentration for the monomer, **4**, and the metallo-dendrimers, **5** and **6**, is presented in Figure 5.

Table 3. Rate and equilibrium data for the reactions between **4** and **5** and py, DMAP, and Br⁻ at 25.0 °C.

	k_n [M ⁻¹ s ⁻¹]	k_{-n} [s ⁻¹]	K_n [M ⁻¹]
Complex 4			
Py	19.9(8)	0.0749(2)	265(9)
DMAP	46.0(2)	0.205(2)	224(5)
Br ⁻	60.8(2)	0.274(4)	222(3)
Complex 5			
Py	22.7(4)	0.105(5)	216(4)
DMAP	50.7(6)	0.255(3)	199(1)
Br ⁻	60.7(2)	0.346(7)	175(6)

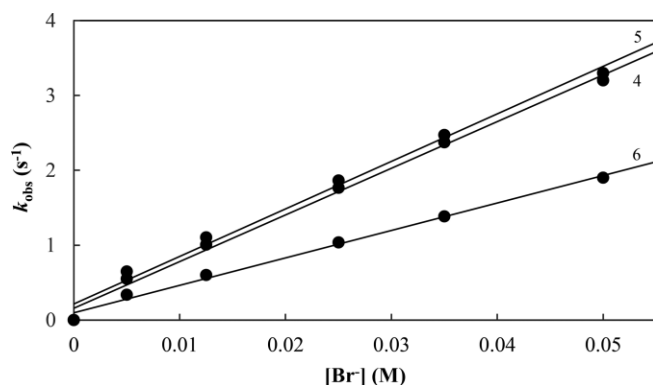


Figure 5. Plot of k_{obs} vs. $[\text{Br}^-]$ for the reaction of **4**, **5** and **6** with Br⁻ at 25.0 °C.

From Figure 5 and Table 3, it can be seen that the second-order constant, k_1 , increases in each case when moving from the monomer, **6**, to the metallodendrimers, **4** and **5**, for each entering ligand used. Furthermore, the k_1 values for **4** and **5** are comparable, with just a slight increase observed for the higher order metallodendrimer in each case. For example, the forward rate constants for the pyridine reactions at 25.0 °C increase from 10.2(1) to 19.9(8) and 22.7(4) M⁻¹ s⁻¹, respectively, when comparing the rates of **6** to **4** and **5**, respectively. This may be attributed to the increased inductive effect, by virtue of the dendritic arms, which influences the electron density around the Re^I metal center. Another reason might be that the metallodendrimers are more rigid than the monomer which has a propyl substituent which could be sterically more hindering as compared to the dendrimers.

The values obtained for the stability constants, K_1 , for the newly formed dendrimer products are in general very similar, but slightly higher than the monomeric complexes as illustrated by K_1 for the formation products of the reactions of **4** [224(5) M⁻¹] and **5** [199(1) M⁻¹] with DMAP compared to that of **6** [95.3(6) M⁻¹]. All these compare well to values obtained for several ranges of *fac*-[Re(CO)₃(Bid)X]^{*n*+} type complexes in literature (Bid = *N,N*-, *N,O*- and *O,O*-bidentate ligands and X = Br⁻, DMAP, py).^[19–24]

The labilizing effect of the bidentate *N,N*-[(pyridine-2-yl)methyl]propan-1-amine ligand in **6** is best illustrated when comparing the value for the second-order rate constant of 0.165(1) M⁻¹ s⁻¹, obtained here for the reaction with Br⁻ ions to that of *fac*-[Re(CO)₃(Bid)(MeOH)] [Bid = 1,10-phenanthroline (phen)/2,2'-bipyridine (bipy)], where values of 0.050(3) M⁻¹ s⁻¹

and 0.042(7) × 10⁻³ M⁻¹ s⁻¹ were obtained for the respective phen and bipy complexes, indicating a factor of 3000 increase in rate. This is to be expected considering that aliphatic amines are strong electron donors.

Conclusions

In summary, first- and second-generation poly(*N,N*-2-picolyl-amino) DAB-PPI dendritic ligands were synthesized via reductive amination reactions and fully characterized. Their corresponding rhenium(I) complexes were synthesized from two rhenium precursors to afford tetra- and octanuclear rhenium(I) metallodendrimers with *fac*-[Re(CO)₃X]^{*n*+} (X = Br and *n* = 0; X = OH₂ and *n* = 1) peripheral entities. In addition, mononuclear complexes were prepared as models for comparison to the larger metallodendrimers. To demonstrate their potential, kinetic studies showed that the second-order rate constants for the reactions of the monomeric complex, **3**, with various entering ligands are almost 2 times lower than what was obtained for similar reactions with its metallodendrimer counterparts. The reasons for this were ascribed to the fact that the monomer has a more flexible substituent which might hinder the substitution process and/or that the dendritic architectures are slightly better electron donors than the corresponding monomer. The preliminary investigation into the activation parameters suggests an I_a type mechanism. The greater significance of the kinetic results is that the dendritic ligands seem to have a stronger labilizing effect than the monomer from which it was derived. This might give an indication of what one can expect for other macromolecules like proteins when coordinated to more than one metal center. However, it is also clear that this work has to be expanded to include more types of ligands and of course, a deeper investigation of the intimate mechanism that drives these substitution processes.

Experimental Section

General: All reagents were purchased from Sigma–Aldrich and used without further purification. 1,4-Diaminobutane poly(propylene amine) octaamine [DAB-PPI-(NH₂)₈] was purchased from SyMO-Chem. *fac*-(Et₄N)₂[Re(CO)₃Br₃]^[35,36] and ligand **L3**,^[37,38] were prepared using literature procedures. All reactions were performed at room temperature using standard Schlenk-line techniques, and the reductive amination reactions were performed under nitrogen gas. Dichloromethane (CH₂Cl₂) was dried using the molecular sieves (Sigma Aldrich, 3 Å beads, 4–8 mesh) and methanol (MeOH) was dried in the Innovative Technology Swagelok® (PS-Micro, PSM-13–564) or over calcium hydride. Nuclear magnetic resonance (NMR) spectra were acquired on a Bruker Ultrashield 400 Plus spectrometer [¹H: 399.95 MHz; ¹³C(¹H): 100.60 MHz] at ambient temperature. All chemical shifts are reported in the standard δ notation of parts per million using tetramethylsilane (TMS) as an internal standard and were referenced relative to the signal of corresponding deuterated solvents. Infrared (IR) spectra were determined, either in the solid state or as Nujol mulls between NaCl discs, with a Perkin–Elmer Spectrum 100 FTIR spectrometer equipped with a SMART iTR ATR unit. Melting points were determined on a Reichert-Jung Thermovar hot-stage microscope and are uncorrected. Elemental analyses were performed using Thermo Flash EA 112 Series com-

bustion analyzer. For selected dendrimers, the analyses include solvent molecules, which are ascribed to the propensity of the dendrimers to encapsulate solvent molecules which are detected after the comprehensive washing steps. Electrospray ionization (ESI⁺) mass spectra were recorded on a Waters API Quattro Micro triple quadrupole mass spectrometer. Electron impact mass spectrometry (EI-MS) was carried out on a JEOL GCmatell mass spectrometer.

Synthesis of Dendritic Ligands (L1 and L2): A solution of DAB-G1-PPI-(NH₂)₄ (0.306 mL, 0.930 mmol for **L1**) or DAB-G2-PPI-(NH₂)₈ (0.360 mL, 0.466 mmol for **L2**) in CH₂Cl₂ (20.0 mL) was added dropwise to a stirred solution of 2-pyridinecarboxyaldehyde (0.355 mL, 3.73 mmol for **L1**; 0.400 mL, 3.73 mmol for **L2**) in dichloromethane (40.0 mL), in the presence of MgSO₄ (ca. 20.0 mg). The reaction mixture was stirred for 24 h at room temperature. The reaction mixture was filtered by gravity and the solvent of the filtrate removed under vacuum to afford a brown crude oil. The brown oil was dissolved in methanol (60.0 mL) and stirred for 30 min, whilst the reaction flask was purged with nitrogen. The crude solution was subsequently reacted with NaBH₄ (0.353 g, 9.33 mmol for **L1**; 0.656 g, 17.3 mmol for **L2**) under nitrogen for 24 h. The excess hydride was quenched with ice-cooled water (20.0 mL) and the H₂O/MeOH mixture was evaporated by rotary evaporation to afford a yellow suspension. The crude product was extracted with CH₂Cl₂ (2 × 30.0 mL) and the organic fractions combined. The solvent was removed under reduced pressure to once again afford a brown oil, and was further purified using reverse-phase column chromatography (H₂O/MeOH, 100:0–50:50 %, 0:100 %). The desired organic fractions were combined and dried with anhydrous MgSO₄, filtered by gravity, and the solvent of the filtrate removed under reduced pressure to afford a brown oil.

L1: Brown oil, yield: 0.190 g, 30.0 %. IR (Nujol between NaCl plates): $\tilde{\nu}$ = 1593 (sharp, pyridyl, C=N), 1377 (sharp, 2° amine, C–N) cm⁻¹. ¹H NMR [(CD₃)₂SO]: δ = 1.42 (m, 4 H NCH₂CH₂CH₂ core), 1.70 (br. qn, 8 H, NCH₂CH₂CH₂N_{branch}), 2.42–2.52 (overlapping m, 12 H, NCH₂CH₂ core, NCH₂CH₂CH₂N_{branch}), 2.69 (br. t, 8 H, NCH₂CH₂CH₂N_{branch}), 2.81 (br. s, 4 H, NH), 3.91 (s, 8 H, Ar_{pyr}-CH₂NH), 7.17 (m, 4 H, CH_{pyr}), 7.33 (br. d, ³J = 7.80 Hz, 4 H, CH_{pyr}), 7.66 (br. td, 4 H, CH_{pyr}), 8.56 (br. d, 4 H, CH_{pyr}) ppm. ¹³C{¹H} NMR [(CD₃)₂SO]: δ = 24.4, 26.7, 47.2, 51.7, 53.4 (CH₂ core, branch), 54.8 (Ar_{pyr}-CH₂N), 121.6, 122.7, 136.2, 148.6 (CH_{pyr}), 159.9 (C_{pyr}) ppm. C₄₀H₆₀N₁₀·2H₂O (717.0200): calcd. C 67.01, H 9.00, N 19.54; found C 66.57, H 8.92, N 19.60; MS (HR-ESI-TOF) *m/z* calculated for C₄₀H₆₀N₁₀: 341.2580, found 341.2581 [M + 2H]²⁺. S₂₅ °C = 0.01 mg/μL in water.

L2: Dark brown oil, yield: 0.89 g, 44.0 %. IR (Nujol between NaCl plates): $\tilde{\nu}$ = 1592 (sharp, pyridyl, C=N), 1377 (sharp, 2° amine, C–N) cm⁻¹. ¹H NMR [(CD₃)₂SO]: δ = 1.28, 1.50, 1.76 (br. m, 36 H, NCH₂CH₂core, NCH₂CH₂1st branch, NCH₂CH₂CH₂NH₂2nd branch), 2.25, 2.34, 2.63 (m, 53 H, NCH₂CH₂2nd branch, NCH₂CH₂core, NCH₂CH₂CH₂N_{1st branch}, NH, CH₂CH₂N_{2nd branch}), 3.74 (s, 16 H, Ar_{pyr}-CH₂N), 7.22 (m, 8 H, Ar_{pyr}), 7.37 (m, 8 H, Ar_{pyr}), 7.67 (m, 8 H, Ar_{pyr}), 8.48 (m, 8 H, Ar_{pyr}) ppm. ¹³C{¹H} NMR [(CD₃)₂SO]: δ = 20.4, 24.2, 27.5, 47.8, 51.5, 51.7 (NCH₂CH₂core, 1st and 2nd branch), 51.9 (Ar_{pyr}-CH₂N), 121.9, 122.8, 134.4, 148.6 (CH_{pyr}), 160.1 (C_{pyr}) ppm. C₈₈H₁₃₆N₂₂·CH₂Cl₂ (1587.1370): calcd. C 67.35, H 8.76, N 19.42; found C 66.91, H 8.76, N 19.18. MS (HR-ESI-TOF) *m/z* calculated for C₈₈H₁₃₆N₂₂: 376.2908, found 376.2898 [M + 4H]⁴⁺. S₂₅ °C = 0.01 mg/μL in water.

Synthesis of fac-[Re(CO)₃Br]-Functionalized Complexes (1–3): fac-(Et₄N)₂[Re(CO)₃Br₃] (0.765 g, 0.993 mmol for **1**; 0.0980 g, 0.128 mmol for **2**; 0.862 g, 1.12 mmol for **3**) was dissolved in MeOH (5.00 mL) and added to a stirring solution of either **L1** (0.169 g, 0.248 mmol for **1**) or **L2** (0.0480 g, 0.0320 mmol for **2**) or **L3** (0.168 g,

1.12 mmol for **3**) in MeOH (5.00 mL). The reagents were stirred at room temp. for 3 h and the product was collected as a precipitate. **1** and **2** were collected as brown precipitates without further purification. **3** was collected as a white fluffy solid and recrystallized from EtOH to afford colorless needles.

fac-[Re(CO)₃(L1)Br] (1): Brown powder, yield: 0.169 g, 19.5 %. IR-ATR: $\tilde{\nu}$ = 2014 (carbonyl, C=O), 1863 (br., carbonyl, C=O), 1609 (s, pyridyl, C=N) cm⁻¹. ¹H NMR [(CD₃)₂SO]: δ = 1.43–1.99 (br. m, 12 H, NCH₂CH₂core, NCH₂CH₂branch), 2.89–3.23 (br. m, 16 H, NCH₂CH₂CH₂N_{branch}, NCH₂CH₂CH₂core), 4.15, 4.46–5.15 (br. m, 12 H, Ar_{pyr}-CH₂N, Ar_{pyr}-CH₂N, NH), 7.54 (m, 4 H, Ar_{pyr}), 7.23 (m, 4 H, Ar_{pyr}), 8.09 (m, 4 H, Ar_{pyr}), 8.76 (br. dd, 4 H, Ar_{pyr}) ppm. ¹³C{¹H} NMR [(CD₃)₂SO]: δ = 24.5, 26.1, 50.9–57.2 (NCH₂CH₂core, 1st branch), 60.2 (Ar_{pyr}-CH₂N), 123.1, 125.7, 140.2, 153.0 (CH_{pyr}), 160.8 (C_{pyr}), 192.4, 196.8, 198.2 (C=O) ppm. C₅₂H₆₀Br₄N₁₀O₁₂Re₄ (2081.93): calcd. C 30.01, H 2.91, N 6.73; found C 30.18, H 3.33, N 6.65; MS (HR-ESI-TOF) *m/z* calcd. for C₅₂H₆₀Br₄N₁₀O₁₂Re₄: 1041.8850, found 1041.9767 [M + 2H]²⁺. MP: 148–151 °C.

fac-[Re(CO)₃(L2)Br] (2): Brown powder, yield: 0.0248 g, 18.0 %. IR-ATR: $\tilde{\nu}$ = 2014 (carbonyl, C=O), 1865 (br., carbonyl, C=O), 1610 (s, pyridyl, C=N) cm⁻¹. ¹H NMR [(CD₃)₂SO]: δ = 1.38–1.86, 3.05–3.39 (br. signals, 40 H, NCH₂CH₂core, NCH₂CH₂CH₂1st and 2nd branch), 4.07 (br. m, 8 H, NH), 4.42 (m, 8 H, Ar_{pyr}-CH₂N), 5.08, (br. d, 8 H, Ar_{pyr}-CH₂N), 7.50 (br. t, 8 H, Ar_{pyr}), 7.66 (br. s, 8 H, Ar_{pyr}), 8.02 (m, 8 H, Ar_{pyr}), 8.71 (m, 8 H, Ar_{pyr}) ppm. ¹³C{¹H} NMR [(CD₃)₂SO]: δ = 25.6, 49.1, 50.8 (NCH₂CH₂core, 1st and 2nd branch), 60.3 (Ar_{pyr}-CH₂N), 123.1, 125.7, 140.3, 152.9 (CH_{pyr}), 160.7 (C_{pyr}), 192.3, 196.7, 198.3 (C=O) ppm. C₁₁₂H₁₃₆Br₈N₂₂O₂₄Re₈ (4303.34): calcd. C 31.26, H 3.19, N 7.16; found C 31.35, H 3.77, N 7.30; MS (HR-ESI-TOF) *m/z* calcd. for C₁₁₂H₁₃₆Br₈N₂₂O₂₄Re₈: 1056.6145, found 1056.5388 [M + 3H – Br]⁴⁺. MP: 140–143 °C.

fac-[Re(CO)₃(L3)Br] (3): Colorless needles, yield: 0.321 g, 57.0 %. IR-ATR: $\tilde{\nu}$ = 2012 (carbonyl, C=O), 1912 (s, carbonyl, C=O), 1875 (s, carbonyl, C=O), 1672 (s, pyridyl, C=N) cm⁻¹. ¹H NMR [(CD₃)₂SO]: δ = 0.93 (t, ³J = 7.41 Hz, 3 H, CH₃CH₂CH₂N), 1.77 (m, 2 H, CH₃CH₂CH₂N), 3.01 (m, 2 H, CH₃CH₂CH₂N), 4.13 (dd, ²J = 15.68, ³J = 8.72 Hz, 1 H, Ar_{pyr}-CH₂N), 4.78 (dd, ²J = 15.72, ³J = 5.08 Hz, 1 H, Ar_{pyr}-CH₂N), 5.03 (br. m, 1 H, NH), 7.51 (t, ³J = 6.06 Hz, 1 H, Ar_{pyr}), 7.71 (d, ³J = 7.84 Hz, 1 H, Ar_{pyr}), 8.02 (td, ³J = 7.75, 1.53 Hz, 1 H, Ar_{pyr}), 8.74 (d, ³J = 5.52 Hz, 1 H, Ar_{pyr}) ppm. ¹³C{¹H} NMR [(CD₃)₂SO]: δ = 11.0 (CH₃CH₂CH₂N), 21.6 (CH₃CH₂CH₂N), 59.7 (CH₃CH₂CH₂N, Ar_{pyr}-CH₂N), 122.6, 125.1, 139.6, 152.4 (CH_{pyr}), 160.4 (C_{pyr}), 191.9, 196.2, 197.7 (C=O) ppm. C₁₂H₁₄BrN₂O₃Re (500.37): calcd. C 28.81, H 2.82, N 5.60; found C 28.92, H 2.77, N 5.42. MS (HR-ESI-TOF) *m/z* calcd. for C₁₂H₁₄BrN₂O₃Re: 421.0562, found 421.0549 [M – Br]⁺. MP: 211–213 °C.

Synthesis of fac-[Re(CO)₃(OH₂)⁺]-Functionalized Complexes (4–6): fac-(Et₄N)₂[Re(CO)₃Br₃] (0.100 g, 0.130 mmol) was dissolved in water (6.00 mL) and the solution was adjusted to pH 2.2 using HNO₃. AgNO₃ (0.066 g, 0.389 mmol) was added to the solution and the suspension was stirred for 24 h to afford fac-[Re(CO)₃(OH₂)₃]NO₃ (0.130 mmol) in solution, this was followed by the removal of AgBr by filtration. Compound **L1** (0.0340 g, 0.0325 mmol for **4**) or **L2** (0.0363 g, 0.0163 mmol for **5**) or **L3** (0.0195 g, 0.130 mmol for **6**) was added to the filtrate and the solution stirred for 10 h at room temp. The product remained in solution and the water was reduced using a freeze drier to afford a colorless or brown suspension.

fac-[Re(CO)₃(L1)(OH₂)⁺] (4): Light-brown suspension, yield: 0.107 g. IR-ATR: $\tilde{\nu}$ = 2020 (carbonyl, C=O), 1881 (s, carbonyl, C=O), 1644 (s, pyridyl, C=N) cm⁻¹. ¹H NMR [(CD₃)₂SO]: δ = 1.71 (br. signal, 4 H, NCH₂CH₂core), 2.09 (br. signal, 8 H, NCH₂CH₂branch), 2.83–3.13 (br. m,

16 H, $\text{NCH}_2\text{CH}_2\text{branch}$, $\text{CH}_2\text{CH}_2\text{NHbranch}$, 4.40, 4.94–4.99 (br. signal, 16 H, $\text{NCH}_2\text{CH}_2\text{core}$, $\text{Ar}_{\text{pyr}}\text{-CH}_2\text{N}$, NH), 7.45–7.53 (m, 8 H, 5-H, 3-H), 7.93 (m, 4 H, 4-H), 8.67 (m, 4 H, 6-H) ppm. $\text{C}_{52}\text{H}_{68}\text{N}_{10}\text{O}_{16}\text{Re}_4\cdot 5\text{HNO}_3$ (2149.06): calcd. C 29.06, H 3.42 N 9.78; found C 29.39, H 3.13, N 9.60; MS (HR-ESI-TOF) m/z calcd. for $\text{C}_{52}\text{H}_{60}\text{N}_{10}\text{O}_{14}\text{Re}_4$: 898.6299, found 898.7490 $[\text{M} + 2\text{H}]^{2+}$. UHPLC ($\text{CH}_3\text{CN}/\text{H}_2\text{O}$, gradient, 20:80 % – 70:30 %, flow rate 1.1 mL/min): $t_{\text{R}} = 6.23$ min.

fac-[Re(CO)₃(L2)(OH₂)]⁺ (5): Brown suspension. IR-ATR: $\tilde{\nu} = 2015$ (carbonyl, C=O), 1863 (s, carbonyl, C=O), 1621 (s, pyridyl, C=N) cm^{-1} . $\text{C}_{112}\text{H}_{152}\text{N}_{22}\text{O}_{32}\text{Re}_8\cdot 15\text{HNO}_3\cdot \text{Et}_4\text{N}$ (4883.66): calcd. C 29.90, H 3.89, N 10.75; found C 29.54, H 3.43, N 10.54. MS (HR-ESI-TOF) m/z calcd. for $\text{C}_{112}\text{H}_{152}\text{N}_{22}\text{O}_{32}\text{Re}_8$: 460.9781, found 461.0756 $[\text{M} + 30\text{H}_2\text{O} + 2\text{Et}_4\text{N}]^{10+}$.

fac-[Re(CO)₃(L3)(OH₂)]⁺ (6): Colorless suspension, yield: 0.674 g. IR-ATR: $\tilde{\nu} = 2022$ (carbonyl, C=O), 1891 (s, carbonyl, C=O), 1624 (s, pyridyl, C=N) cm^{-1} . ^1H NMR [$(\text{CD}_3)_2\text{SO}$]: $\delta = 0.83$ (t, $^3J = 7.46$ Hz, 3 H, $\text{CH}_3\text{CH}_2\text{CH}_2\text{N}$), 1.59 (m, 2 H, $\text{CH}_3\text{CH}_2\text{CH}_2\text{N}$), 2.94 (t, $^3J = 7.71$ Hz, 2 H, $\text{CH}_3\text{CH}_2\text{CH}_2\text{N}$), 4.26 (br. m, 2 H, $\text{Ar}_{\text{pyr}}\text{-CH}_2\text{N}$), 7.47–7.55 (m, 2 H, H5, Ar_{pyr}), 7.96 (td, $^3J = 7.77$, 1.73 Hz, 1 H, Ar_{pyr}), 8.52 (d, $^3J = 5.13$ Hz, 1 H, Ar_{pyr}) ppm. $\text{C}_{12}\text{H}_{16}\text{N}_2\text{O}_4\text{Re}$ (438.48): calcd. C 32.87, H 3.86, N 6.39; Found C, 32.23; H, 3.45; N, 7.00. MS (HR-ESI-TOF) m/z calcd. for $\text{C}_{12}\text{H}_{16}\text{N}_2\text{O}_4\text{Re}$: 421.0562, found 421.0560 $[\text{M} - \text{H}_2\text{O}]^+$.

X-ray Crystallography

Diffraction data was collected on a Bruker ApexII 4 K CCD diffractometer using Mo- K_{α} (0.71073 Å) and ω -scans at 100 K. All reflections were merged and integrated with SAINT-PLUS^[39] and corrected for Lorentz, polarization, and absorption effects using SADABS.^[40] Both structures were solved by the heavy atom method and refined through full-matrix least-squares cycles using SHELXL-97^[41] as part of the WinGX^[42] package with $\Sigma(|F_o| - |F_c|)^2$ being minimized. All non-H atoms were refined with anisotropic displacement parameters, while hydrogen atoms were constrained to parent atom sites using a riding model {aromatic C–H = 0.95 Å [$U_{\text{iso}}(\text{H}) = 1.2U_{\text{eq}}$]; aliphatic C–H = 0.98 Å [$U_{\text{iso}}(\text{H}) = 1.5U_{\text{eq}}$]}. The graphics were obtained with the visual crystal structure information system software DIAMOND.

CCDC 1472296 (for **3**) contains the supplementary crystallographic data for this paper. These data can be obtained free of charge from The Cambridge Crystallographic Data Centre.

Kinetic Studies

The kinetic measurements were initially performed on a Varian Cary 50 Conc UV/Vis spectrophotometer equipped with a Julabo F12-mV temperature cell regulator (accurate within 0.1 °C). The kinetic reactions of coordinated methanol substitution were observed to occur rapidly under UV/Vis. Thus, rapid kinetic reactions (reaction half-lives shorter than 20 seconds) were monitored at four different temperatures 5.0, 15.0, 25.0, and 35.0 °C (accurate within 0.1 °C) on Kinet AsystTM Hi-Tech Scientific M300 SHU-615X2 Stopped Flow Spectrophotometer attached to a Julabo MPV thermostat water bath (accurate within 0.1 °C). The third generation stopped-flow system has a thermostatic sample handling unit and can be operated in the diode-array mode with a dead time < 5.00 microseconds, yielding 400 nm spectral width scans at < 5.00 microseconds per complete scan.

All the kinetic runs were performed under pseudo-first-order conditions with the ligand in large excess in each case. Least-squares analyses were performed on the absorbance vs. time data obtained from the kinetics runs to appropriate functions using MicroMath Scientist. The solid lines in the figures represent computer least-squares fits of data, while experimental values are represented as

individual points, denoted by selected symbols. Activation parameters were determined from Eyring plots.

Acknowledgments

The authors would like to thank the Nuclear Technologies in Medicine and the Biosciences Initiative (NTEMBI), a national technology platform developed and managed by the South African Nuclear Energy Corporation (NECSA) and funded by the Department of Science and Technology, South Africa. Financial support from the University of Cape Town (UCT), the University of the Free State, the National Research Foundation (NRF) of South Africa, and South African Nuclear Energy Corporation (NECSA) is gratefully acknowledged and thanked for several short term exchange visits between the various laboratories.

Keywords: Rhenium · Dendrimers · Kinetics · Ligand effects

- [1] P. Govender, B. Therrien, G. S. Smith, *Eur. J. Inorg. Chem.* **2012**, 2853–2862.
- [2] S. Langereis, A. Dirksen, T. M. Hackeng, M. H. P. van Genderen, E. W. Meijer, *New J. Chem.* **2007**, 31, 1152–1160.
- [3] Z.-X. Liu, Y. Feng, Z.-Y. Zhao, Z.-C. Yan, Y.-M. He, X.-J. Luo, C.-Y. Liu, Q.-H. Fan, *Chem. Eur. J.* **2014**, 20, 533–541.
- [4] D. F. Baban, L. W. Seymour, *Adv. Drug Delivery Rev.* **1998**, 34, 109–119.
- [5] D. Astruc, E. Boisselier, C. Ornelas, *Chem. Rev.* **2010**, 110, 1857–1959.
- [6] C. Ghobril, G. Lamanna, M. Kueny-Stotz, A. Garofalo, C. Billotey, D. Felder-Flesch, *New J. Chem.* **2012**, 36, 310–323.
- [7] H. B. Agashe, A. K. Babbar, S. Jain, R. K. Sharma, A. K. Mishra, A. Asthana, M. Garg, T. Dutta, N. K. Jain, *Nanomed.: Nanotechnol. Biol. Med.* **2007**, 3, 120–127.
- [8] M. C. Parrott, S. R. Benhabbour, C. Saab, J. A. Lemon, S. Parker, J. F. Valliant, A. Adronov, *J. Am. Chem. Soc.* **2009**, 131, 2906–2916.
- [9] S. Hecht, J. M. J. Frechet, *Angew. Chem. Int. Ed.* **2001**, 40, 74–91; *Angew. Chem.* **2001**, 113, 76.
- [10] Y. Zhang, X. Xu, Y. Sun, Y. M. Shen, *Chin. J. Chem.* **2010**, 28, 2447–2450.
- [11] A. J. North, D. J. Hayne, C. Schieber, K. Price, A. R. White, P. J. Crouch, A. Rigopoulos, G. J. O’Keefe, H. Tochon-Danguy, A. M. Scott, J. M. White, U. Ackermann, P. S. Donnelly, *Inorg. Chem.* **2015**, 54, 9594–9610.
- [12] P. J. Blower, *Dalton Trans.* **2015**, 44, 4819–4844.
- [13] R. Alberto, R. Schibli, W. R. U. Abram, A. P. Schubiger, *Coord. Chem. Rev.* **1999**, 190–192, 901–919.
- [14] R. Alberto, *J. Organomet. Chem.* **2007**, 692, 1179–1186.
- [15] R. Alberto, H. Braband, H. W. P. N’Dongo, *Curr. Radiopharm.* **2009**, 2, 254–267.
- [16] R. Alberto, R. Schibli, A. Egli, P. A. Schubiger, U. Abram, T. A. Kaden, *J. Am. Chem. Soc.* **1998**, 120, 7987–7988.
- [17] T. R. Hayes, B. B. Kasten, C. L. Barnes, P. D. Benny, *Dalton Trans.* **2014**, 43, 6998–7001.
- [18] S. Mundwiler, M. Kundig, K. Ortner, R. Alberto, *Dalton Trans.* **2004**, 1320–1328.
- [19] A. Brink, H. G. Visser, A. Roodt, *J. Coord. Chem.* **2011**, 64, 122–133.
- [20] A. Brink, H. G. Visser, A. Roodt, *Inorg. Chem.* **2013**, 52, 8950–8961.
- [21] A. Brink, H. G. Visser, A. Roodt, *Polyhedron* **2013**, 52, 416–423.
- [22] A. Brink, H. G. Visser, A. Roodt, *Inorg. Chem.* **2014**, 53, 12480–12488.
- [23] M. Schutte, G. Kemp, H. G. Visser, A. Roodt, *Inorg. Chem.* **2011**, 50, 12486–12498.
- [24] M. Schutte, A. Roodt, H. G. Visser, *Inorg. Chem.* **2012**, 51, 11996–12006.
- [25] R. Alberto, R. Schibli, A. Egli, P. A. Schubiger, W. A. Herrmann, G. Artus, U. Abram, T. A. Kaden, *J. Organomet. Chem.* **1995**, 493, 119–127.
- [26] S. Hochreuther, R. Puchta, R. van Eldik, *Inorg. Chem.* **2011**, 50, 12747–12761.
- [27] M. S. Davies, J. W. Cox, S. J. Berners-Price, W. Barklage, Y. Qu, N. Farrel, *Inorg. Chem.* **2000**, 39, 1710–1715.
- [28] A. Egli, K. Hegetschweiler, R. Alberto, U. Abram, R. Schibli, R. Hedinger, V. Gramlich, R. Kissner, P. A. Schubiger, *Organometallics* **1997**, 16, 1833–1840.

- [29] N. Lazarova, S. James, J. Babich, J. Zubieta, *Inorg. Chem. Commun.* **2004**, 7, 1023–1026.
- [30] M. Cohn, T. R. J. Hughes, *J. Biol. Chem.* **1962**, 237, 176–181.
- [31] H. M. MacConnell, *J. Chem. Phys.* **1958**, 28, 430.
- [32] M. Prudencio, J. Rohovec, J. A. Peters, E. Tocheva, M. J. Boulanger, M. E. P. Murphy, H.-J. Hupkes, W. Kusters, A. Impagliazzo, M. Ubbink, *Chem. Eur. J.* **2004**, 10, 3252–3260.
- [33] P. V. Grundler, L. Helm, R. Alberto, A. E. Merbach, *Inorg. Chem.* **2006**, 45, 10378–10390.
- [34] J. F. G. A. Jansen, E. M. E. de Brabander-van den Berg, E. W. Meijer, *Science* **1994**, 266, 1226–1269.
- [35] R. Alberto, A. Egli, U. Abram, K. Hegetschweiler, V. Gramlich, P. A. Schubiger, *J. Chem. Soc., Dalton Trans.* **1994**, 2815–2820.
- [36] R. Alberto, R. Schibli, P. A. Schubiger, U. Abram, T. A. Kaden, *Polyhedron* **1996**, 15, 1079–1089.
- [37] D. Ma, F. Lu, T. Overstreet, D. E. Milenic, M. W. Brechbiel, *Nucl. Med. Biol.* **2002**, 29, 91–105.
- [38] P. Bandyopadhyay, S. Jha, S. K. I. Ali, *J. Agric. Food Chem.* **2009**, 57, 9780–9786.
- [39] G. M. Sheldrick in *SAINT*, Bruker AXS Inc., Madison, WI, USA, **2006**.
- [40] G. M. Sheldrick in *SADABS*, University of Göttingen, Germany, **1997**.
- [41] G. M. Sheldrick, *Acta Crystallogr., Sect. A* **2008**, 64, 112–122.
- [42] L. J. Farrugia, *J. Appl. Crystallogr.* **1997**, 30, 565.

Received: June 5, 2017